

Low-contrast resolution in volumetric x-ray CT—Analytical comparison between conventional and spiral CT

Ge Wang^{a)} and Michael W. Vannier

Department of Radiology, University of Iowa, Iowa City, Iowa 52242

(Received 9 April 1996; accepted for publication 26 November 1996)

Spiral/helical computed tomography (CT) was introduced to scan an anatomical volume in a single breath-hold for better temporal resolution as compared to conventional CT. Recently, it was established that given an x-ray dose, spiral CT also allows better longitudinal high-contrast resolution due to retrospective reconstruction. In spiral CT, full scan with interpolation (FI) and half-scan with interpolation (HI) are limited by the degraded slice sensitivity profile and increased image noise, respectively. We combined these two interpolation methods for a desirable balance. This new interpolation method, FI+HI, was shown to produce 4% lower image noise standard deviation than conventional CT, without loss of longitudinal bandwidth according to one-tenth-cutoff and mean-square-root measures. The analytic model of image noise was validated in a water phantom experiment. Our findings suggest the superiority of spiral CT over conventional CT in terms of both low-contrast resolution and high-contrast resolution. © 1997 American Association of Physicists in Medicine. [S0094-2405(97)01103-6]

Key words: spiral/helical computed tomography (CT), image quality, slice sensitivity profile (SSP), noise, low-contrast resolution

I. INTRODUCTION

Spiral/helical computed tomography (SCT) was initially developed to improve temporal resolution by continuous and simultaneous patient translation, gantry rotation, and data acquisition.¹⁻⁴ SCT requires that planar projection sets be synthesized from raw projection data via interpolation. Among various methods, linear interpolation is usually preferred due to its efficiency and performance.^{2,5} Typical linear interpolation techniques include full scan with interpolation (FI) and half-scan with interpolation (HI). In the FI method, a set of planar projection data in a 360° angular range is obtained via linearly interpolating neighboring raw projection data at the same orientation, hence the raw data involved span a 720° angular range. The HI method utilizes redundancy of raw data, interpolates neighboring raw data at opposite directions, and thus reduces the angular range from 720° to 360° plus two fan angles. Recently, it was established that for a given x-ray dose and with the HI method, SCT allows a substantially wider longitudinal bandwidth as compared to conventional CT (CCT); in other words, SCT allows substantially better high-contrast resolution.⁶⁻¹⁰

CCT being the standard, it is well known that SCT with the FI method decreases image noise, while SCT with the HI method increases image noise.^{2,5,11} On the other hand, the FI method degrades the slice sensitivity profile (SSP) significantly more than the HI method.^{2,5} As a result, it appears that SCT would suffer from either a poorer high-contrast resolution (with FI) or a poorer low-contrast resolution (with HI). However, we will show in this paper that SCT can be better than CCT in both longitudinal bandwidth and image noise characteristics; that is, SCT can provide superior high- and low-contrast resolution *simultaneously*.

II. INTERPOLATION METHOD FI+HI

Since both the FI and HI methods have their advantages and disadvantages, we attempt to balance them. As shown in Fig. 1, from a SCT raw dataset and at a given longitudinal position, two transaxial images can be reconstructed using the FI and HI methods, respectively. Then, these two images are averaged to produce a new reconstructed image. Because both interpolation and reconstruction processes are linear with either FI or HI, the averaging operation may be moved into the interpolation process in the raw projection data domain for better computational efficiency. The resultant interpolation method is denoted as FI+HI.

A. Longitudinal bandwidths

The SSP completely describes longitudinal resolution, and possesses the same information content as the transfer function (TF) that is essentially the Fourier transform of the SSP. It is more convenient to work in the Fourier domain,⁹ where the spatial resolution is typically parametrized as the bandwidth. Both the one-tenth cutoff and mean-square-root measures⁹ can be used for bandwidth quantification.

Fourier transform $F(u)$ of a one-dimensional function $f(x)$ is defined as

$$F(u) = \int_{-\infty}^{\infty} f(x) e^{-i2\pi ux} dx. \quad (1)$$

Based on the established formulas for the SSPs with FI and HI,^{5,9} the Fourier transform $P_{FI+HI}(u)$ of the SSP with FI+HI can be shown to be as follows:

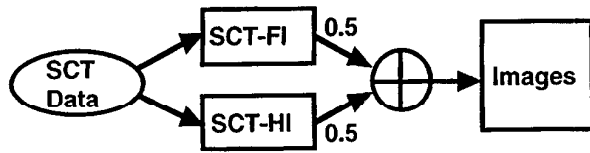


Fig. 1. FI+HI method. In FI+HI, a reconstructed image is the average of the two corresponding images reconstructed using FI and HI, respectively. The averaging operation can be directly implemented in spiral CT data interpolation.

$$P_{FI+HI}(u) = \frac{1}{2} \left[\text{sinc}^3(\pi Du) + \text{sinc}^2\left(\frac{\pi Du}{2}\right) \text{sinc}(\pi Du) \right], \quad (2)$$

where both table increment and detector collimation are the same and denoted by D ; also, the reconstruction interval between adjacent transaxial slices is assumed to be sufficiently small.

For $P_{FI+HI}(u)$, the one-tenth-cutoff bandwidth can be determined by setting it to 0.1 and solving the equation on the interval of the main lobe. The mean-square root of a Fourier power spectrum is defined as $\sqrt{\int_0^\infty u^2 |F(u)|^2 du / \int_0^\infty |F(u)|^2 du}$. Bandwidth values with FI+HI were computed using the software system MATHEMATICA™ after setting $D=1$, and are listed in Table I along with those of CCT, FI, and HI.⁹ It can be observed in Table I that *as compared to CCT, spiral CT with FI+HI is equivalent or better in terms of the mean-square-root and one-tenth-cutoff bandwidth measures, respectively.*

B. Image noise

Based on an idealized model (an additive white projection noise in a parallel-beam format), it was established¹¹ that SCT image noise variance is, *on average*, proportional to raw projection noise variance averaged according to the corresponding interpolation weighting function, if the average projection noise variance is independent of the detector position [Eq. (10) in Ref. 11]. Our analytic predictions were consistent to experimental data measured at the gantry isocenter.²

Using the same methodology,¹¹ the average raw projection noise variance can be estimated for the FI+HI method. As shown in Fig. 2, the table increment per half-scan is assumed to be one; at any transaxial slice position $z \in [0,1]$, four raw projection rays $\alpha, \beta, \gamma,$ and δ are involved in interpolation. Both FI and HI interpolation functions are weighted

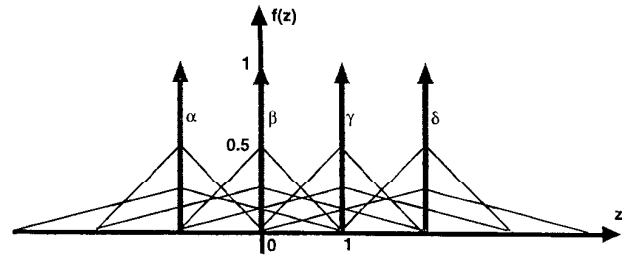


Fig. 2. Spiral CT data interpolation using FI+HI. To synthesize a planar projection data set at z in $[0,1]$, rays α, β, γ and δ are involved, where neighboring rays are in opposite orientations, the table increment per half-scan is 1, and FI and HI weighting functions are represented by shorter and taller triangles, respectively.

by 0.5 and assigned to each raw projection ray. In $[0,1]$, there are six contributing interpolation weighting functions:

$$f_{\alpha,FI}(z) = -\frac{z}{8} + \frac{1}{8}, \quad (3)$$

$$f_{\beta,FI}(z) = -\frac{z}{8} + \frac{1}{4}, \quad (4)$$

$$f_{\beta,HI}(z) = -\frac{z}{2} + \frac{1}{2}, \quad (5)$$

$$f_{\gamma,FI}(z) = \frac{z}{8} + \frac{1}{8}, \quad (6)$$

$$f_{\gamma,HI}(z) = \frac{z}{2}, \quad (7)$$

$$f_{\delta,FI}(z) = \frac{z}{8}, \quad (8)$$

where the first subscript denotes the ray with which an interpolation function is associated, and the second denotes the type of interpolation. The average raw projection noise variance can be computed as

$$\bar{\sigma}^2 = \int_0^1 [f_{\alpha,FI}^2(z) + (f_{\beta,FI}(z) + f_{\beta,HI}(z))^2 + (f_{\gamma,FI}(z) + f_{\gamma,HI}(z))^2 + f_{\delta,FI}^2(z)] dz = \frac{11}{24}. \quad (9)$$

The noise values in projection and image domains for CCT, FI, HI, and FI+HI are summarized in Table II, where values for CCT, FI, and HI are from Ref. 11, and a half-scan reconstruction formula is assumed. Since full-scan projection data are actually available in CCT and FI, and reconstruction is done using a half-scan algorithm, the full-scan data are first

TABLE I. Bandwidth values for CCT, SCT FI, HI, and FI+HI. It was assumed that both detector collimation and table feed were 1 cm.

Bandwidth	CCT	FI	HI	FI+HI
One-tenth cutoff	0.500	0.63	0.838	0.758
Mean-square root	0.256	0.215	0.297	0.256

TABLE II. Noise variance and standard deviation values for CCT, SCT FI, HI, and FI+HI.

Noise	CCT	FI	HI	FI+HI
Var. in Projection	0.500	0.333	0.667	0.458
Var. in Images	1.000	0.667	1.333	0.917
St. D. in Image	1.000	0.817	1.155	0.957

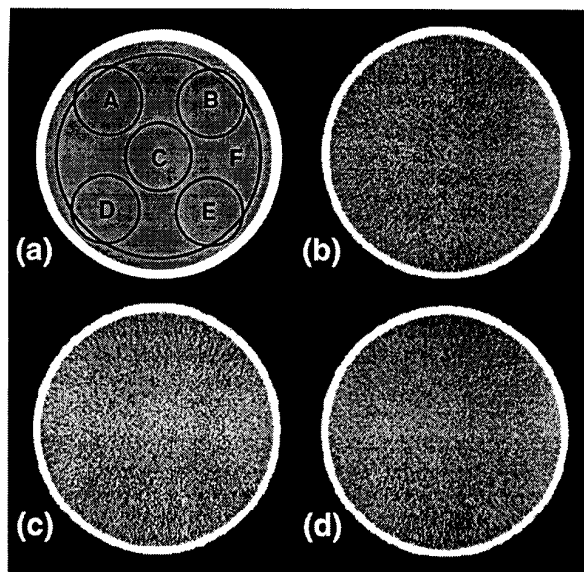


FIG. 3. Water phantom images. (a) Six regions of interest for noise measurement, (b) image reconstructed using FI, (c) image reconstructed using HI, and (d) averaged image from images (b) and (c).

transformed into half-scan data. As a consequence, the corresponding projection noise variance values listed in Table II are the actual ones divided by 2. It can be observed in Table II that *FI+HI* reduces the image noise standard deviation by more than 4% compared to *CCT*.

III. EXPERIMENTAL VALIDATION

The SSPs with FI and HI were previously validated.^{2,3,5} Hence, the SSP with FI+HI must be the average of those with FI and HI, *by construction*. On the other hand, validation of image noise prediction for FI+HI is important, because of the approximate nature of the mathematical treatment involved.

A spiral CT scanner (Siemens Somatom PLUS-S, Siemens Medical Systems, Iselin, NJ) was employed in our experiment. A research spiral CT software package is available for the scanner to perform either FI or HI.^{3,5} A CT performance phantom (76-410-4130DT, Nuclear Associates, Carle Place, NY) was transformed into a water phantom after

removal of internal parts. The cylindrical water phantom was made of acrylic plastic with outside and inside diameters of 21.59 and 20.32 cm, respectively.

The phantom was spirally scanned with 4 mm detector collimation and 4 mm table feed for a 108 mm coverage, and reconstructed at two randomly selected table positions using FI and HI, respectively. Reconstructed images at the same table position were then averaged to synthesize two corresponding FI+HI images. Figure 3(a) shows six regions of interest (ROI) for measurement of image noise, Figs. 3(b)–3(d) are images reconstructed at the first selected table position using FI, HI, and FI+HI, respectively. Table III lists noise standard deviations of the six ROIs in the image reconstructed at the first selected table position, along with experimental and theoretical ratios of the noise standard deviations. Although the ratio between standard deviations of image noise produced by FI+HI and HI, respectively, has not been measured previously, the standard deviation ratio of image noise produced by FI and HI is widely known. Noise standard deviation ratios FI/HI and (FI+HI)/HI were computed for all ROIs and both table positions. The mean ratios FI/HI and (FI+HI)/HI of the five small ROIs are 0.691 and 0.823, respectively, *for either table position*, being very close to measured values from large ROIs, and consistent with theoretical values 0.704 and 0.829, as shown in Table III. This demonstrates that our image noise formulation for the FI+HI method is valid.

IV. DISCUSSION AND CONCLUSION

Low-contrast image resolution quantifies the system capability to reveal small local attenuation changes in the human body, and is critically important for some clinical applications, such as lesion detection. Low-contrast resolution is affected by both image noise and image blurring. While image noise is primarily quantified by variance, image blurring can be described by a system bandwidth. Our results have suggested that *SCT* with FI+HI is superior to *CCT* in terms of both longitudinal bandwidth and image noise; in other words, *SCT may provide better low-contrast resolution than CCT for a given x-ray dose without compromising high-contrast resolution*.

Our FI+HI method was constructed via linearly combining FI and HI with equal weights. An arbitrary linear combination of FI and HI would cover a continuous spectrum for *SCT* raw data interpolation, and give the following TF:

TABLE III. Noise standard deviations (in HU) of the six regions of interest in the transaxial images reconstructed at the first selected table position, and ratios of noise standard deviations.

	A	B	C	D	E	F	Mean ratios of regions A–E	Theoretic ratios at image isocenter
St. D. with FI	8.951	9.182	10.509	8.557	8.971	9.284		
St. D. with HI	13.751	14.033	15.255	11.724	12.312	13.512		
St. D. FI+HI	11.114	11.359	12.560	9.803	10.313	11.103		
FI/HI	0.651	0.654	0.689	0.730	0.729	0.687	0.691	0.704
(FI+HI)/HI	0.808	0.809	0.823	0.836	0.838	0.822	0.823	0.829

$$P_{\text{FI+HI}}(u) = \alpha \operatorname{sinc}^3(\pi Du) + (1 - \alpha) \times \operatorname{sinc}^2\left(\frac{\pi Du}{2}\right) \operatorname{sinc}(\pi Du), \quad (10)$$

where $\alpha \in [0, 1]$. Other schemes for linear or nonlinear interpolation could be better in specific applications.¹²

Strictly speaking, both the SSP and image noise are spatially variant.^{10,13} By definition, such variations for FI+HI can be obtained by appropriately averaging those for FI and HI, respectively. It has been widely accepted in practice that the SSP and image noise at the isocenter of the field of view can be used as the overall measures, and our work reported here was based on the isocenter formulas. Therefore, our statement on low-contrast resolution should be interpreted in the average sense.

ACKNOWLEDGMENTS

The authors thank anonymous reviewers for the constructive comments, B. Brunnsden and R. Knapp for important technical support. The research spiral CT software package was provided by Professor W. A. Kalender of the University of Erlangen, Dr. A. Polacin and Dr. E. Klotz of the Siemens AG, Germany. This work was supported in part by grants from the Whitaker Foundation (The Biomedical Engineering Program) and the National Institutes of Health (NIDCD R03 DC02798 and NIDDKD R29 DK50184).

⁰Electronic-mail: ge-wang@uiowa.edu

¹Y. Bresler and C. J. Skrabacz, "Optimal interpolation in helical scan computed tomography," in Proc. ICASSP 3, 1472-1475 (1989).

²C. R. Crawford and K. F. King, "Computed tomography scanning with simultaneous patient translation," *Med. Phys.* **17**, 967-982 (1990).

³W. A. Kalender, W. Seissler, E. Klotz, and P. Vock, "Spiral volumetric CT with single-breath-hold technique, continuous transport, and continuous scanner rotation," *Radiology* **176**, 181-183 (1990).

⁴I. Mori, "Computerized tomographic apparatus utilizing a radiation source," U.S. Patent Number 4,630,202, 1986.

⁵A. Polacin, W. A. Kalender, and G. Marchal, "Evaluation of section sensitivity profiles and image noise in spiral CT," *Radiology* **185**, 29-35 (1992).

⁶W. A. Kalender, A. Polacin, and C. Süß, "A comparison of conventional and spiral CT: An experimental study on detection of spherical lesions," *J. Comput. Assist. Tomogr.* **18**, 167-176 (1994).

⁷W. A. Kalender, "Thin-section three-dimensional spiral CT: Is isotropic imaging possible?," *Radiology* **197**, 578-580 (1995).

⁸G. Wang, J. A. Brink, and M. W. Vannier, "Theoretical FWTM values in helical CT," *Med. Phys.* **21**, 753-754 (1994).

⁹G. Wang and M. W. Vannier, "Longitudinal resolution in volumetric x-ray CT—Analytical comparison between conventional and helical CT," *Med. Phys.* **21**, 429-433 (1994).

¹⁰G. Wang and M. W. Vannier, "Spatial variation of section sensitivity profile in helical CT," *Med. Phys.* **21**, 1491-1497 (1994).

¹¹G. Wang and M. W. Vannier, "Helical CT image noise—Analytical results," *Med. Phys.* **20**, 1635-1640 (1993).

¹²J. Hsieh, "A general approach to the reconstruction of x-ray helical computed tomography," *Med. Phys.* **23**, 221-229 (1996).

¹³C. R. Crawford, K. F. King, and H. Hu, "Helical CT noise reduction with optimized starting angles," *Radiology* **193**, 170 (1994).